CIRP Annals - Manufacturing Technology xxx (2017) xxx–xxx

Contents lists available at ScienceDirect

CIRP Annals - Manufacturing Technology

journal homepage: http://ees.elsevier.com/cirp/default.asp

Chatter avoidance in cutting highly flexible workpieces

Gabor Stepan (2)[a,*], Adam K. Kiss[a], Behnam Ghalamchi[b], Jussi Sopanen[b], Daniel Bachrathy[a]

[a] Department of Applied Mechanics, Budapest University of Technology and Economics, Budapest, Hungary
[b] Department of Mechanical Engineering, Lappeenranta University of Technology, Lappeenranta, Finland

ARTICLE INFO

Keywords:
Chatter
Finite element method (FEM)
Flexible workpiece

ABSTRACT

Robust stability analysis of turning is presented for flexible workpiece. The varying dynamic properties due to the material removal process is modelled by means of finite element method. The Frequency Response Function is traced along tool position. The results show significant change in the natural frequency and modal stiffness, which have strong influence on regenerative chatter vibration. Different sections of the multiple-parameter stability lobe diagram are presented and validated with experimental results. The robust stable parameters of initial diameter and chip width are identified for which no chatter occurs along the whole tool position for any spindle speed.

1. Introduction

Regenerative chatter in turning machines is a type of self-excited oscillation that can be caused by flexibility in the machine, cutting tool and/or workpiece. Vibration analysis in machining operation is important for accurate prediction and elimination of possible chatter, and for effective planning of the cutting process.

In turning operation, the surface regenerative effect can be described as a time delayed system where the position of the cutting edge in the previous revolution affects the chip evolution (see the detailed mechanical models in Refs. [1,2]).

Several studies on the corresponding chatter vibrations are summarized in Ref. [3]. It is well known that cutting force properties as well as the dynamical characteristics of the machine and the workpiece have major effects on chatter stability for flexible systems (e.g. turbine blade, thin shaft). FEM is a natural choice for modelling thin-walled workpieces [4,5], which is proper method for tracing the changing dynamical properties due to material removal. In Ref. [4], still, only static deformation is taken into account.

In Ref. [6], an approach is presented to simulate flexible workpiece vibration during 5-axis milling. In Ref. [7], simulation is presented for turning thin tubular parts with tracing chatter frequency variation.

Natural frequencies and mode shapes obtained with FEM must be verified with modal testing [8]. However, this work did not consider the change of workpiece geometry during machining, therefore, the corresponding stability chart did not provide a conservative estimate of chatter-free cutting.

In the case of milling processes, the varying geometry of a plate-type workpiece was modelled by structural modification and receptance coupling between FE models in Refs. [5,9]. Tool position dependent 3D stability charts are developed in Refs. [10–12], which give opportunity to design varying spindle speed along tool position to avoid chatter [13,14]. Similar observations are obtained for thin workpieces in Ref. [15].

The above mentioned methods do not provide robust parameter set for which the whole cutting process is stable. This study presents stability analysis of the turning process for varying workpiece geometry related to material removal: the changing dynamical properties of the system are taken into account in the stability calculations. The Frequency Response Function (FRF) is generated as a function of the tool position, which leads to multi-parameter stability charts. Robust stability criteria are formed for stable turning independent of the spindle speed and/or the tool position. The proposed method is verified by laboratory tests.

2. Turning process

In order to perform the stability calculation, the mechanical model of the turning process of a flexible workpiece is considered as shown in Fig. 1. The governing equation assumes the form

$$\mathbf{M}\ddot{\mathbf{y}}(t) + \mathbf{C}\dot{\mathbf{y}}(t) + \mathbf{K}\mathbf{y}(t) = \mathbf{Q}(t). \tag{1}$$

The workpiece deformation is described by the generalized coordinate vector $\mathrm{y}(t) = [y_1(t), y_2(t), \ldots, y_n(t)]^{\mathrm{T}}$, and the dynamical parameters of the workpiece are defined in the mass, damping and stiffness matrices as **M**, **C** and **K**, respectively. The resultant cutting-force applied at the current tool position s at the corresponding excited eth coordinate y_e is included in the general force $\mathbf{Q}(t) = [0, \ldots, 0, F_y(t), 0, \ldots, 0]^{\mathrm{T}}$ (see Fig. 1). The cutting force is described by the widely used linear force model [2], where the magnitude of the cutting force is linearly proportional to the chip thickness $h(t)$:

$$F_y(t) = K_y w h(t). \tag{2}$$

Here, K_y is the cutting force coefficient and w is the chip width. In the case of an ideally rigid tool and workpiece, the chip thickness

* Corresponding author.
E-mail address: stepan@mm.bme.hu (G. Stepan).

http://dx.doi.org/10.1016/j.cirp.2017.04.054
0007-8506/© 2017 Published by Elsevier Ltd on behalf of CIRP.

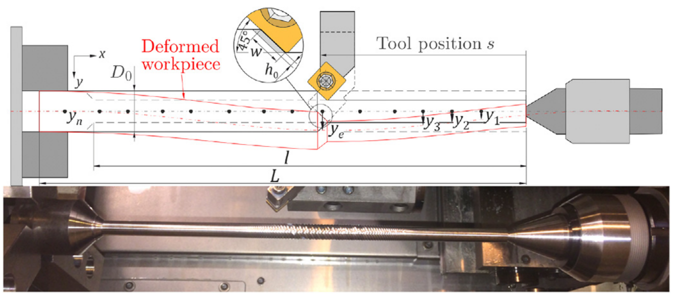

Fig. 1. Mechanical model of the cutting process and the flexible workpiece. Dots refer to schematic representation of FEM nodes.

would be constant, but in cases with flexibility the surface regeneration effect [1] must be taken into account where the instantaneous chip thickness is influenced by the present and the delayed relative position between the tool and workpiece as follows:

$$h(t) = h_0 + y_e(t-\tau) - y_e(t). \tag{3}$$

The general solution $\mathbf{y}(t)$ in Eq. (1) can be described by a small perturbation $\boldsymbol{\xi}(t)$ around the static deformation $\mathbf{y}_{\mathbf{st}}$ as $\mathbf{y}(t) = \mathbf{y}_{\mathbf{st}} + \boldsymbol{\xi}(t)$. The corresponding governing equation

$$\mathbf{M}\ddot{\boldsymbol{\xi}}(t) + \mathbf{C}\dot{\boldsymbol{\xi}}(t) + \mathbf{K}\boldsymbol{\xi}(t) = \boldsymbol{\kappa}(\boldsymbol{\xi}(t-\tau) - \boldsymbol{\xi}(t)) \tag{4}$$

describes the stability properties of the stationary turning process, where $\boldsymbol{\kappa}$ is a matrix with zero elements except

$$\kappa_{e,e} = K_y w. \tag{5}$$

In the case of flexible workpiece, it is crucial to trace the variation of the mass, damping and stiffness matrices as the geometry varies due to the material removal process. In the subsequent section, the FE model and its modal coordinate reduction is presented for the varying geometry.

3. Dynamics of the workpiece

The flexibility of the workpiece in Fig. 1b is modelled by means of using Timoshenko beam element with proportional damping in the FEM formulation. The constraints are often modelled as pinned joints or clamped ends, however, the measured FRF showed that the compliance and the damping of the bearing system of the turning machine are not negligible. Scanning Laser-Doppler Vibrometer (SLDV PSV-500) was used to make non-contact measurements on the response of the workpiece excited by modal hammer. Fig. 2a presents the first natural frequencies and the corresponding peak values of the direct receptance functions at the excited positions s after the material segment with length s was removed. The stiffness and the damping parameters of the bearing system were obtained by means of a fitting algorithm based on the measured natural frequencies and mode shapes (the optimized parameters are given in Table 1.).

Fig. 2a shows that the workpiece dynamics can significantly change during the cutting operation in two different ways. One corresponds to the motion of the cutting tool, which is taken into account by means of the mode shapes. The other one relates to the effect of the material removal process, which leads to varying

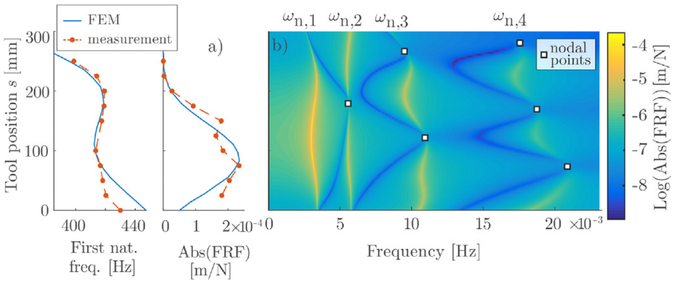

Fig. 2. (a) Measured and calculated values of the first natural frequency and the corresponding peak values of the receptance functions; (b) tool position dependent FRF function together the nodal points.

Table 1
Applied workpiece and technological parameters.

Initial diameter	42 mm	Bearing stiffness	1.1×10^7 N/m
Total length L	363 mm	FEM node number n	40
Cutting length l	308 mm	Chip thickness h_0	0.2 mm
Material	34CrNiMo6	Spindle speed Ω	3500 rpm
Density	7800 kg/m^3	Spec cutting force coeff K_y	85 MPa
Elasticity	220 GPa	Rake angle	26.5°
Bearing damping	10 Ns/m	Clearance angle	45°

workpiece geometry and correspondingly varying dynamical parameters, primarily the natural frequency of the workpiece.

Based on Eq. (1), the FRF can be predicted using the matrices **M**, **C** and **K**. The use of full-size matrices would be computationally expensive [16] and in most cases only the first few modes are relevant to the stability analysis [15]. In this study, modal reduction technique is applied to decrease the number of degrees of freedom (DoF). Decoupled equations of motion for each modal coordinate $\chi_i(\omega, s)$ in the frequency domain can be written as [17]

$$-\omega^2\chi_i(\omega,s) + i\omega 2\zeta_i(s)\omega_{n,i}(s)\chi_i(\omega,s) + {\omega_{n,i}}^2(s)\chi_i(\omega,s) = \phi_i(\omega), \tag{6}$$

where $\phi_i(\omega)$ is the generalized force corresponding to the ith mode shape, $\omega_{n,i}(s)$ is the natural angular frequency, and $\zeta_i(s)$ is the modal damping of the ith mode shape, $i = 1,2, \ldots, m$, where m ($<n$) is the number of modes considered to be relevant. Note, that these parameters depend on the tool position coordinate s due to the varying geometry, which is updated at each node as the tool passes.

With a FE based model, the variation of the FRF can be identified for each node of the FE model. Due to the special form of matrix $\boldsymbol{\kappa}$ in Eq. (4), only a single element in the FRF matrix is relevant for the stability calculation. This direct FRF $H_{e,e}(\omega, s)$ of the excited point is defined in Eq. (7) as a function of the tool position s:

$$H_{e,e}(\omega,s) = \sum_{i=1}^{m} \frac{T_{e,i}^2(s)}{-\omega^2 + i\omega 2\zeta_i(s)\omega_{n,i}(s) + {\omega_{n,i}}^2(s)}, \tag{7}$$

where $T_{e,i}(s)$ is the element of the ith mass-normalized mode shape at the excited coordinate. In Fig. 2b, the amplitude of $H_{e,e}(\omega, s)$ is presented for different tool positions. Clearly, the variation of the peaks is proportional to the corresponding mode shapes. The figure also shows that the workpiece is relatively stiff near both ends of the workpiece, and furthermore, it is dynamically stiff at the nodal points of the corresponding mode shapes, as well. The measured values and the FEM resulted FRF of the mechanical model show good correlation (see Fig. 2a), which supports our selected damping factors and bearing stiffness parameters.

4. Stability analysis

In the following section, the stability boundaries of the regenerative turning process are determined based on the D-subdivision method [18] via the real and imaginary parts of the characteristic equation:

$$D(\Omega, w, s, D_0, \omega) = \sum_{i=1}^{m} \frac{T_{e,i}^2(s)}{-\omega^2 + i\omega 2\zeta_i(s)\omega_{n,i}(s) + {\omega_{n,i}}^2(s)} \boldsymbol{\kappa}\left(1 - e^{-i\omega\tau}\right) = 0 \tag{8}$$

Usually, the stability chart is presented in the plane of spindle speed Ω and chip width w (see black curves in Fig. 3) at fixed tool position s and diameter D_0, however, in the case of a flexible workpiece, it is recommended to extend this lobe structure along the tool position resulting a 3D stability chart (see Fig. 3) [5,10–14,19]. Furthermore, the initial diameter of the shaft can be analysed, which leads to a 4-dimensional parameter space as displayed in Eq. (8). Even a 3D chart is hard to visualise and so it would be difficult for a machine operator to select chatter-free parameter combinations.

A selected roughing operation at a certain chip width w (with given initial diameter D_0) defines the horizontal section of the 3D

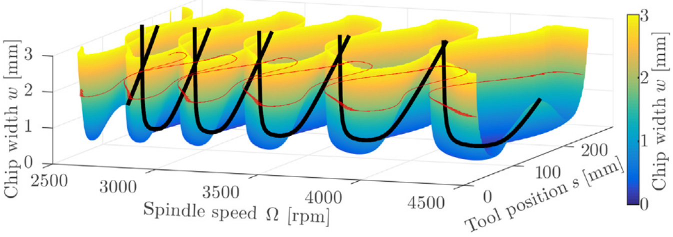

Fig. 3. Tool position dependent 3D stability chart for initial diameter D_0 = 16 mm; black: traditional lobe structure at tool position s = 150 mm; red: stability boundaries at chip width w = 1.75 mm.

chart in Fig. 3, which is represented by red curves. The top view is plotted in Fig. 4a, from which a constant spindle speed can be chosen (see blue dashed vertical line) to avoid chatter along the whole workpiece. If only lower spindle speeds are available, then a controlled spindle speed variation is needed along the tool position (curved dotted-dashed line in Fig. 4a) [13,14], which is a challenging problem. At low spindle speeds, where the lobing effect is not significant, unstable stability islands merge and only the minimum and maximum tool positions (connected by green lines) have practical relevance. These tool position points define the shaded green area in Fig. 4a, also called the robust stable area, which is independent of the selected spindle speeds [5].

It should be noted that this map is valid for a given initial diameter D_0, and therefore, it cannot be used in the designing process for roughing operations where the oversize of the workpiece is removed with several consecutive immersions. Therefore, this map is extended along the fourth parameter D_0 of Eq. (8) for some given spindle speeds (Ω = 3600, 3700, 3800 rpm), as shown in Fig. 4b. The envelope of these curves is the same robust stable limit as described above. In the corresponding green area, the cutting process is always stable; outside the green area, that is, inside the envelope, the turning process can be stable or unstable depending not only on the initial diameter D_0, but also on the spindle speed Ω. The larger the diameter, the stiffer the shaft, and therefore, the larger the (green) robust areas along the tool position. Above a critical diameter D^* (orange square in Figs. 4 and 5) no chatter vibration occurs along the entire tool position.

The effect of the chip width w on the robust area is presented in the parameter space of the tool position s and the initial diameter D_0 in Fig. 5a. Fig. 5b shows only the critical diameter D^* as a function of chip width w, where the dark green area is robustly stable against the spindle speed and tool position. This diagram can be useful from the practical point of view, because, the most productive chip width can be selected from the green area close to the robust stability limit for each diameter during the roughing operation. In this case, the machining is stable for any spindle speed along the whole tool position.

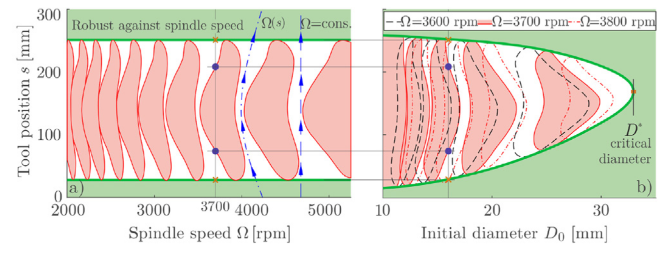

Fig. 4. (a) Stability boundaries for chip width w = 1.75 mm and initial diameter D_0 = 16 mm. Constant (blue dashed line) and controlled (blue dotted-dashed line) spindle speed to avoid chatter; (b) stability boundaries as a function of initial diameter D_0 for chip width w = 1.75 mm; green area: spindle speed independent robust stability domain.

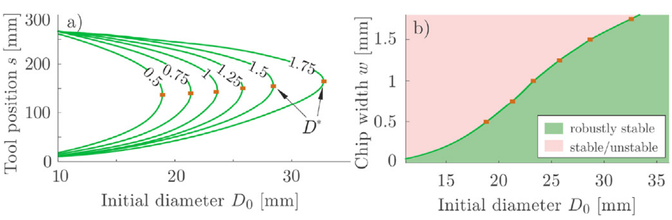

Fig. 5. a) Spindle speed independent robust stability limits (green lines) and the corresponding critical diameters (orange squares) for different chip widths w; b) green: spindle speed and tool position independent robust stability domain, red: stable or unstable domain depending on the spindle speed and the tool position.

5. Experimental validation

To validate the above theoretical results, several cutting tests were performed in a Doosan Puma 2500Y CNC lathe with a Sandvic SNMM 12 04 12-PR 4215 insert in PAFANA hR 111.26 2525 tool holder on a 34CrNiMo6 workpiece. The technological parameters are presented together with geometry and material properties in Table 1. The parameter K_y was selected according to Ref. [2] for the parameters: friction angle 31.6°, maximum shear stress 613 MPa, and shear angle 42.45°.

During the cutting tests, a series of initial diameter and chip width combinations were used for each immersions. The vibrations were measured using an industrial acoustic microphone (Shure Prologue 14 L) and piezo accelerometer (PCB Piezotronic 353B03). The spectrogram of the measured vibration signal clearly presents the locations of the initialisation of chatter and its sudden vanishing. In addition, the machined surface topography was analysed with laser scanning after each cutting process. The start and end points of the evolving chatter vibration could also be localised properly by means of the measured surface pattern (see Fig. 6).

It should be noted that the chatter frequency ω_c varied according to the changing natural frequency during the measurement. This effect can be traced from the spectrogram and from the different slopes of the scanned surface; the tangents of the slopes are determined using the ratio of ω_c/Ω [20]. These are highlighted with blue lines in Fig. 6a.

This phenomenon can also be detected in the numerical simulation of the non-smooth turning model that is combined with the fly-over effect, while the dynamical properties are varied during the simulation [21,22]. The simulated surface pattern is presented in Fig. 6d. In addition, the stability lobe number can also be identified as the number of the waves along the circumference of the workpiece [23].

The validation of the mechanical model is presented for 2 different sets of measurement parameters (chip width w = 1 and 2 mm). The corresponding stability diagram and the detected stable and unstable regions are presented in Fig. 7 in the plane of tool position s and the initial diameter D_0 for spindle speed Ω = 3500 rpm. As Fig. 7a shows, 2 stable regions can be found between the predicted unstable islands, where chatter vibration is avoided along the full tool path. The measurements at diameter D_0 = 15, 18 mm clearly validate this characteristic (Fig. 7a), while at D_0 = 13, 16 mm, the starting and vanishing points of the measured chatter vibration coincide with the predicted stability boundary. (This case corresponds to the dashed vertical line in Fig. 4 in the plane of the technological parameters Ω and s.)

Based on engineering expectations, the occurrence of unstable operations would be predicted at the middle (soft) region of the

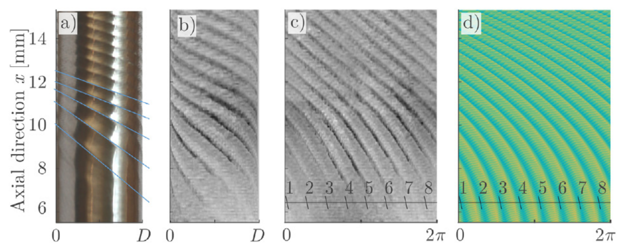

Fig. 6. Chatter marks on the workpiece around the starting location near lobe #8 for parameters: D = 16 mm, w = 2 mm; photo of the surface a); laser scanned surface profile: spatial b), unfolded c); simulated chatter mark d) in case of varying dynamics.

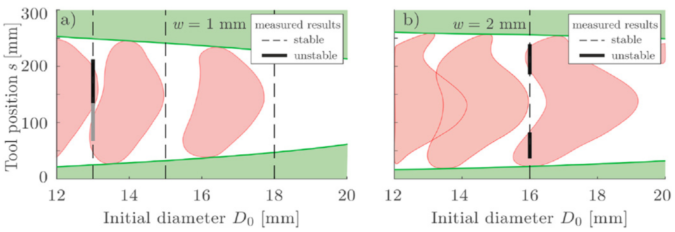

Fig. 7. Stable (thin dashed line) and unstable (thick lines) workpiece segments based on the localised chatter marks together with the corresponding computed stability domains (parameters: Table 1).

shaft. This prediction is valid only at low spindle speed, where the lobing effect does not play a role due to the merging of unstable islands and only the spindle speed independent of the robust stable range is relevant. However, a special case was also measured at large spindle speed, where two unstable areas appeared, which were separated by a stable domain in between at the middle of the shaft (see Fig. 7b with D_0 = 16 mm). The calculated stability boundaries show good correlation with the measured ones, even for the special cases of Fig. 7. It can thus be claimed that the mechanical model is validated and the results, presented in Fig. 5b, are applicable in practice.

It should, however, be borne in mind, that for small workpiece diameters large static deformations $\mathbf{y}_{st}$ take place, which can lead to an offset error in the diameter. This error can be significant and must be included in the modelling, since it modifies the resultant diameter and changes the chip width for the next immersion [24]. However, these can be implemented in the presented model and the whole roughing operation can be described by regenerating the matrices **M**, **C** and **K** for the modified new geometry. A test case is presented in Fig. 8, where the resultant diameters of a simulated roughing operation for chip width w = 1.5 mm are plotted together with the corresponding measured values. The computed curves give a satisfactory prediction for the diameter offset, except where the surface marks, especially the ones caused by chatter, strongly influence the diameter measurement.

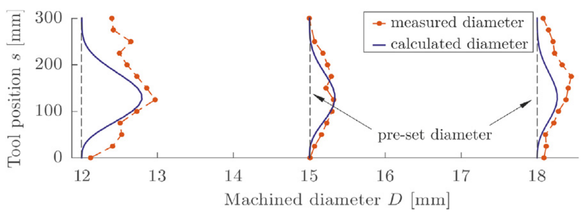

Fig. 8. Measured and simulated resultant diameters caused by static deformations for simulated roughing operation for chip width w = 1.5 mm.

6. Conclusion

It is well-known that varying dynamic properties of a workpiece can have significant impact on the stability chart of turning processes [3]. In the present study, the changing natural frequency and dynamic stiffness (FRF) are traced with an optimised FEM with using bearing parameters tuned to modal tests. New extended 4D multi-parameter stability charts are introduced together with their 2D sections, which have practical relevance for the design of robustly stable turning processes. These results support the technology design to identify those parameters where the turning process is efficient and still robustly stable for any cutting speed and any tool position along the flexible workpiece while maximal chip width is applied (see Fig. 5).

In case the maximization of the material removal rate requires even further improvement in the applied technology, another properly selected section of our 4D stability chart guides the engineer to design a varying spindle speed along the tool path (see Fig. 4). This methodology provides a hierarchy of cutting parameter selections depending on the production requirements.

The model and the corresponding methodology were validated by the analysis of the chatter marks including their start and end locations and the related instability lobe numbers (see Figs. 6–7).

Since the offset error in diameter is also included in the model, the evaluation of the surface error can also be predicted even for non-uniform diameters of complex workpieces, and its compensation can be designed for selected roughing operations.

It is still left for future research to optimize the possible variation of the cutting parameters through the intricate instability lobe structure of the identified 4D stability chart (see, for example, two realizations of $\Omega(s)$ marked with blue curves in Fig. 4). The application of further parameters, like the applied compressive force at the tail-stock, provides further possibilities to improve the efficiency of chatter-free turning.

Acknowledgements

The research was funded by the European Research Council under the European Union's Seventh Framework Programme (FP7/2007-2013) ERC Advanced grant agreement No. 340889 and by Tekes—Finnish Funding Agency for Technology & Innovation.

References

[1] Tobias SA (1965) *Machine-Tool Vibration*, Blackie & Sons Ltd., London.
[2] Altintas Y (2012) *Manufacturing Automation*, University Press Cambridge, UK.
[3] Munoa J, Beudaert X, Dombovari Z, Altintas Y, Budak E, Brecher C, Stepan G (2016) Chatter Suppression Techniques in Metal Cutting. *CIRP Annals—Manufacturing Technology* 65(2):785–808.
[4] Budak E, Altintas Y (1995) Modeling and Avoidance of Static Form Errors in Peripheral Milling of Plates. *International Journal of Machine Tools and Manufacture* 35(3):459–476.
[5] Budak E, Tunç L, Alan S, Ogüven HN (2012) Prediction of Workpiece Dynamics & Its Effects on Chatter Stability in Milling. *CIRP Annals* 61(1):339–342.
[6] Biermann D, Kersting P, Surmann T (2010) A General Approach to Simulating Workpiece Vibrations During Five-Axis Milling of Turbine Blades. *CIRP Annals* 59(1):125–128.
[7] Gerasimenko A, Guskov M, Duchemin J, Lorong P, Gouskov A (2015) Variable Compliance-Related Aspects of Chatter in Turning Thin-Walled Tubular Parts. *Procedia CIRP* 31:58–63.
[8] Mahdavinejad R (2005) Finite element analysis of machine and workpiece instability in turning. *International Journal of Machine Tools and Manufacture* 45 (7–8):753–760.
[9] Tuysuz O, Altintas Y (2017) Frequency Domain Updating of Thin-Walled Workpiece Dynamics Using Reduced Order Substructuring Method in Machining. *Journal of Manufacturing Science and Engineering* 139(7):071013. 16 pages.
[10] Bravo U, Altuzarra O, López Lacalle LN, Sánchez JA, Campa FJ (2005) Stability Limits of Milling Considering the Flexibility of the Workpiece & the Machine. *International Journal of Machine Tools and Manufacture* 45(15):1669–1680.
[11] Thevenot V, Arnaud L, Dessein G, Cazenave LG (2006) Influence of Material Removal on the Dynamic Behavior of Thin-walled Structures in Peripheral Milling. *Machining Science and Technology* 10:275–287.
[12] Song Q, Ai X, Tang W (2011) Prediction of Simultaneous Dynamic Stability Limit of Time–variable Parameters System in Thin-walled Workpiece High-speed Milling Processes. *International Journal of Advanced Manufacturing Technology* 55(9):883–889.
[13] Seguy S, Campa FJ, Lopez de Lacalle LN, Arnaud L, Dessein G, Aramendi G (2008) Toolpath dependent stability lobes for the milling of thin-walled parts. *International Journal of Machining and Machinability of Materials* 4(4):377–392.
[14] Campa F, de Lacalle LL, Celaya A (2011) Chatter Avoidance in the Milling of Thin Floors with Bull-Nose End Mills: Model & Stability Diagrams. *International Journal of Machine Tools and Manufacture* 51(1):43–53.
[15] Kiss AK, Bachrathy D, Stepan G (2016) *Surface Error and Stability Chart of Beam-Type Workpiece in Milling Processes*, ASME IDETC, Charlotte, NC, USA. http://dx.doi.org/10.1115/DETC2016-59940.
[16] Law M, Altintas Y, Phani AS (2013) Rapid Evaluation and Optimization of Machine Tools with Position-dependent Stability. *International Journal of Machine Tools and Manufacture* 68:81–90.
[17] Ewins DJ (2000) *Modal Testing, Theory, Practice, & Application*, 2nd edition. Wiley Hoboken, USA.
[18] Stepan G (1989) *Retarded Dynamical Systems: Stability & Characteristic Functions*, Longman Scientific & Technical, New York, USA.
[19] Schmitz TL, Burns TJ, Ziegert JC, Dutterer B, Winfough WR (2006) Tool Length-Dependent Stability Surfaces. *Machining Science and Technology* 8(3):377–397.
[20] Lorong P, Larue A, Duarte AP (2011) Dynamic Study of Thin Wall Part Turning. *CIRP International Conference on Modeling of Machining Operations Advances Materials Research* 223:591–599.
[21] Dombovari Z, Barton DAW, Wilson RE, Stepan G (2010) On the Global Dynamics of Chatter in Orthogonal Cutting Model. *International Journal of Non-Linear Mechanics* 46(1):330–338.
[22] Molnar TG, Insperger T, Stepan G (2016) Estimation of Safe Chatter-free Technological Parameter Regions for Machining Operations. *Procedia CIRP* 46:464–467.
[23] Altintas Y, Weck M (2004) Chatter Stability of Metal Cutting & Grinding. *CIRP Annals* 53(2):619–642.
[24] Kiss AK, Bachrathy D, Stepan G (2016) Cumulative Surface Location Error for Milling Processes Based on Tool-tip Frequency Response Function. *Procedia CIRP* 46:323–326.